# Supporting Information

## Molecularly engineered dual-network eutectogel electrolytes for high-loading and stable zinc-iodine batteries

Ling Wang[1,2], Jinpeng Guan[2], Na Li[1,*], Jing Li[1], Zhaoyu Wang[1], Jin Yin[1], Yi-Lin Liu[3], Maolin Yu[4], Yongbiao Mu[2,*], Zetao Chen[2], Yuwei Li[2], Jianxiong Xu[4,*], Lin Zeng[2,*]

[1]School of Materials Science and Engineering, Hunan University of Technology, Zhuzhou 412007, China

[2]Department of Mechanical and Energy Engineering, Southern University of Science and Technology, Shenzhen 518055, P. R. China

[3]College of Mechanical Engineering, University of South China, Hengyang 421001, P. R. China

[4]School of Biological Science and Medical Engineering, Hunan Key Laboratory of Biomedical Nanomaterials and Devices, Hunan University of Technology, Zhuzhou 412007, PR China

*Correspondence email: lina@hut.edu.cn(Na Li); muyb2021@mail.sustech.edu.cn (Yongbiao Mu); xujx@hut.edu.cn (Jianxiong Xu); zengl3@sustech.edu.cn (Lin Zeng)

# 1. Experimental Section

## 1.1 Materials

[2-(Methacryloyloxy)ethyl]dimethyl-(3-sulfonopropyl)ammonium hydroxide **(DMAPS) monomer, N-hydroxyethyl acrylamide (HEAA) monomer, Diethyl glycol dimethyl acrylate (TEGDA), photoinitiator, Irgacure 2959 Glycerol(Gly), Choline chloride (ChCl), Zinc trifluoromethanesulfonate($Zn(OTf)_2$), Iodide ($I_2$) and Zinc iodide ($ZnI_2$) was purchased from Macklin. Active carbon (AC) was purchased from Kuraray China Co. Zn foil, Cu foil, and stainless-steel wire were purchased from Shenzhen Kejing Technology.**

## 1.2 Synthesis of PHEAA/PDMAPS(HD) double network synthesis of deep eutectic solvent (DES) hydrogel electrolytes (HD-DESs)

ChCl and Gly were mixed at a molar ratio of 1:2 and stirred in an oil bath at 100 ℃ for 1 h to obtain a clear DES solvent. Subsequently, DMAPS and HEAA monomers were added into the DES at a mass ratio of 1:10 and stirred at room temperature for 30 min. Then, 1 wt% photoinitiator Irgacure 2959 and 0.1 wt% crosslinker TEGDA were added, with the volume ratio of DES to HEAA maintained at 1:2. The mixture was stirred at room temperature until complete dissolution. The resulting gel precursor solution was immediately injected into a mold with a thickness of 0.5 mm and irradiated under UV light for 2 min to form the gel, yielding the PDMAPS/PHEAA eutectogel. **The PDMAPS/PHEAA eutectogel was immersed in a 2M $Zn(OTf)_2$ solution until swelling equilibrium was achieved, resulting in the PDMAPS/PHEAA eutectogel electrolyte, designated as HD-DESs. For the HD double-network hydrogel electrolyte, the low-eutectic solvent was replaced with an equal volume of deionized water. Similarly, the PHEAA single-network hydrogel electrolyte was prepared by substituting the low-eutectic solvent with an equal volume**

**of deionized water and adding only HEAA monomer, with all subsequent steps following the same procedure as for HD-DESs.** After full absorption of the $Zn(OTf)_2$ electrolyte solution, the resulting gel electrolyte used for cell assembly had a thickness of approximately 0.6 mm**.**

## 1.3 Preparation of $I_2$@AC

**In a normal procedure, $I_2$ and AC in a weight ratio of 1:1 was placed in a sealed Teflon liner. Then, the sealed Teflon liner was heated at 120 ℃ for 6 h. Finally, the Teflon liner was opened and continued to be heated at 80 ℃ for 3 h to remove the unstable iodine, which was named $I_2$@AC.**

## 1.4 Preparation of high-loading iodine cathodes.

**Mix $I_2$@AC, conductive carbon, and PTFE adhesive in a mass ratio of 90:5:5. After fibrillation, the mixture was pressed into a self-supporting electrode film, which was then attached onto a titanium mesh current collector and punched into circular electrodes with a diameter of 12 mm. The iodine loading was adjusted by controlling the mass and thickness of the electrode film, yielding cathode electrodes with iodine loadings of 19.0 and 28.1 mg $cm^{-2}$.**

## 1.5 Electrochemical measurements

Electrochemical measurements were conducted using coin-type cells. **The working electrodes were prepared by mixing 80 wt.% $I_2$@AC, 10 wt.% Acetylene Black and 10 wt.% polyvinylidene fluoride (PVDF) in N-methyl pyrrolidone (NMP) to form a slurry, and then the slurry was coated on Titanium mesh, the mass loading of $I_2$ was about 0.8-1.2 mg $cm^{-2}$. The coin cell CR2032 was assembled by the prepared electrode as the cathode, Zn foil as the anode, the hydrogel electrolyte was used as both electrolyte and separator. Neware battery measurement system for constant current charge/discharge testing of cells in the voltage range of 0.6-1.6 V. Cyclic voltammograms**

**(CV) and electrochemical impedance spectra (EIS) were conducted on a CHI660E electrochemical workstation.**

**The ionic conductivity of the hydrogel electrolyte was calculated according to Equation 1:**

$$\delta = \frac{L}{R_S A} \#(1)$$

**where L, $R_S$, and A represent the thickness, resistance, and area of the electrolyte, respectively.**

**Utilizing the Arrhenius equation (equation 2) to calculate the activation energy:**

$$\frac{1}{R_{ct}} = Ae^{-\frac{E_a}{RT}} \#(2)$$

**where $R_{ct}$, A, R, and T denote the charge transfer impedance, frequency factor, gas constant, and absolute temperature respectively.**

**The zinc ion transference number (t+) of different gel electrolytes was measured using Zn symmetric cells based on Equation 3:**

$$t_{Zn^{2+}} = \frac{I_S(\Delta V - I_0 R_0)}{I_0(\Delta V - I_S R_S)} \#(3)$$

**Here, a constant polarization voltage of 10 mV was applied, where $I_0$ and $I_S$ represent the initial current and steady-state current, respectively, while $R_0$ and $R_S$ denote the initial resistance and steady-state resistance.**

## 1.6 Material characterization

**Fourier-transform infrared spectroscopy (FTIR) and Raman spectroscopy (Horiba LabRAM HR Evolution, 532 nm laser) were used to analyze chemical structures. The freezing point of hydrogel electrolytes was measured using differential scanning calorimetry (DSC, TA**

**Instruments). Mechanical properties were assessed using a universal testing machine (Instron 5967) at a tensile rate of 10 mm $min^{-1}$.**

**A series of the products were tested by X-ray diffraction (XRD) on a Bruker D8 Advanced X-ray Diffractometer (Cu-Kα radiation: λ=0.15406 nm) for the phase analysis. X-ray photoelectron spectroscopy (XPS) analysis was carried out with an ESCALAB 250Xi instrument using Al Kα radiation (1486.6 eV). Scanning electron microscope (SEM, Hitachi SU-8230) and laser scanning confocal microscopy (LSCM, Zeiss LSM 800) were employed for studying the morphology of the samples at an acceleration voltage of 5.0 kV. High-resolution transmission electron microscopy (HRTEM) images and energy dispersive X-ray spectroscopy mapping images were captured on a Tecnai G2 F30 transmission electron microscopy at an acceleration voltage of 300 kV. High-angle annular dark-field scanning transmission electron microscopy (HAADF-STEM) was performed on TEM Titan Themis. Additionally, Brunauer-Emmett-Teller (BET) and Barrett-Joyner-Halenda (BJH) tests were conducted on the Autosorb IQ3 instrument.**

## 1.7 Computational Methods

**Molecular dynamics (MD) simulations were conducted using the Forcite module with the COMPASS III force field in Materials Studio[1]. Van der Waals and Coulomb interactions were considered, using atom-based and Ewald methods with a 12.5 Å cutoff. The motion equations were integrated at a 1 fs time step. Following energy minimization, each system underwent a 100 ps relaxation period under periodic boundary conditions in the NPT ensemble (Pressure = 1 atmosphere, Temperature = 298.0 K), using the Nose thermostat and Berendsen barostat for stabilization of temperature, potential, and total energy. After equilibrium, a 500 ps simulation**

**in the NVT ensemble was performed for trajectory analysis, radial distribution function (RDF), and coordinate number (CN) analysis.**

**Quantum chemical calculations were conducted using density functional theory (DFT). All DFT computations were performed employing the DMol3 method[2]. This method utilizes rapidly convergent three-dimensional numerical integrations to compute matrix elements within the Ritz variational approach. A double numerical basis set with polarization functions on all atoms except hydrogen, known as the DND basis set, was utilized. For geometry optimizations, the generalized gradient approximation (GGA) functional BLYP was applied. The convergence criteria for these optimizations included thresholds of $1 \times 10^{-5}$ Ha for energy, 0.004 Ha/Å for gradient, and 0.005 Å for displacement. Additionally, a self-consistent field (SCF) density convergence threshold of 1 × 10−5 Ha was employed. The Pulay direct inversion of iterative subspace (DIIS) technique was used to enhance SCF convergence.**

## 2. Supporting Figures

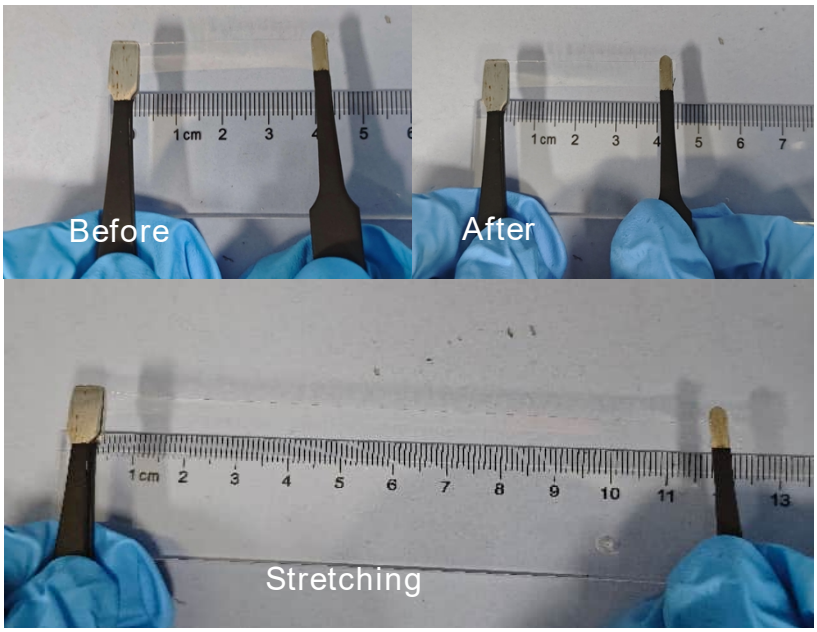


**Figure S1.** HD-DESs Gel Stretch Optical Images.

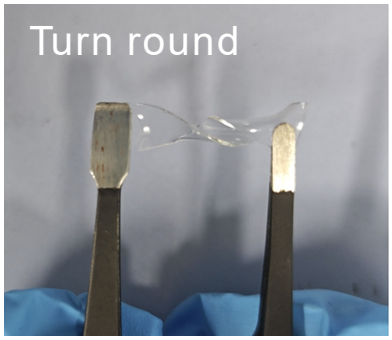


**Figure S2.** HD-DESs optical images of gel torsion.

**The dimensions of the gel strip used for the mechanical-flexibility demonstration were approximately 40 mm × 8 mm × 0.3 mm (length × width × thickness)**


**Figure S3. Optical images of gel electrolyte under a) −40 ℃, b) 25 ℃ and c) 60 ℃.**

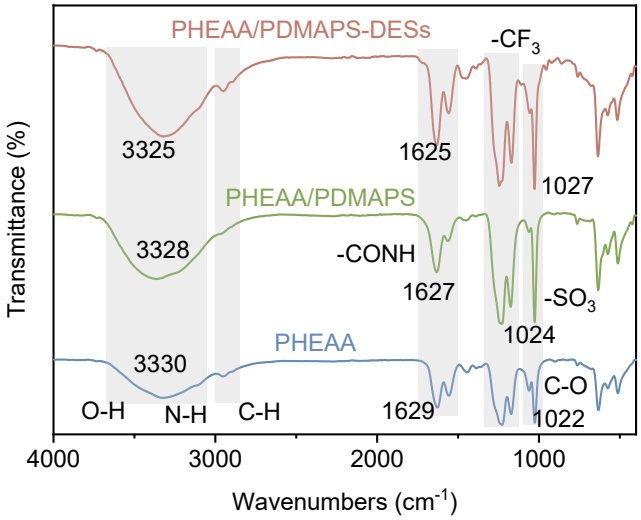


**Figure S4. The FT-IR curves of different gel electrolytes.**

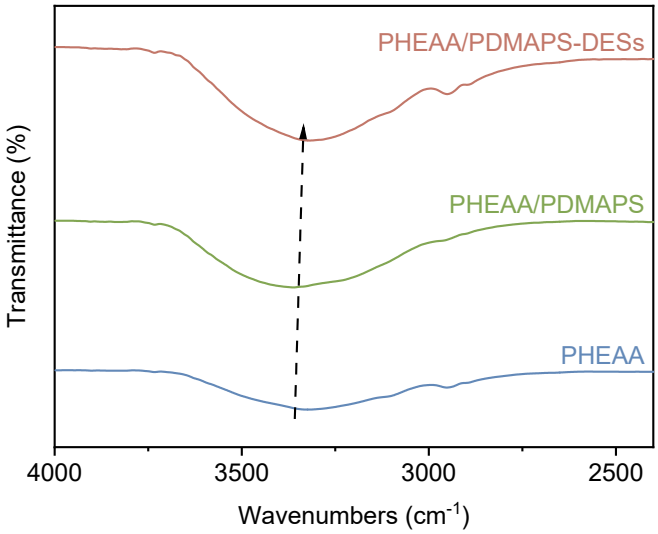


**Figure S5. The FT-IR curves of different gel electrolytes for -OH.**

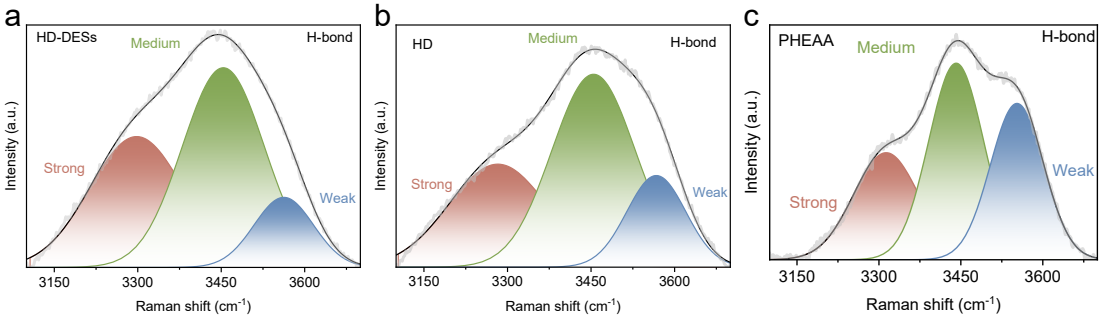


**Figure S6. Deconvoluted Raman spectra of a) HD-DESs electrolytes, b) HD and c) PHEAA in the O−H stretching region.**

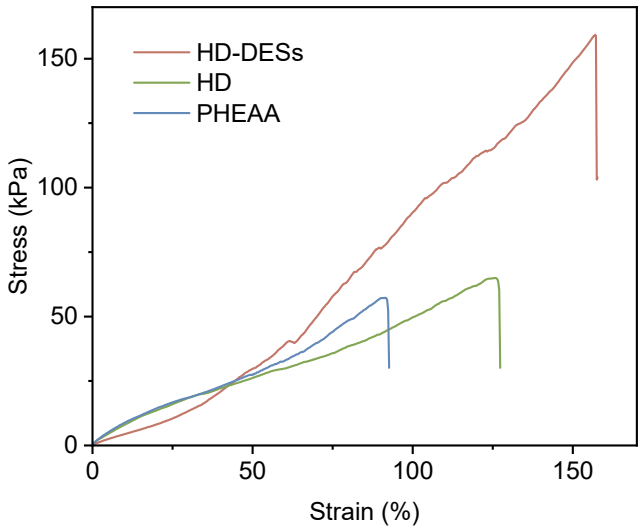


**Figure S7. The stress-strain curves of different gels.**

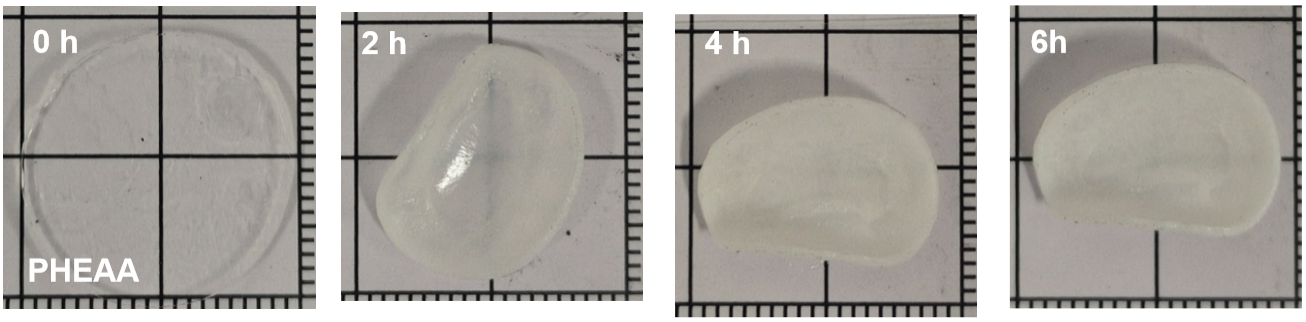


**Figure S8. Optical images of PHEAA electrolytes from 0h to 6 h at 60 °C.**

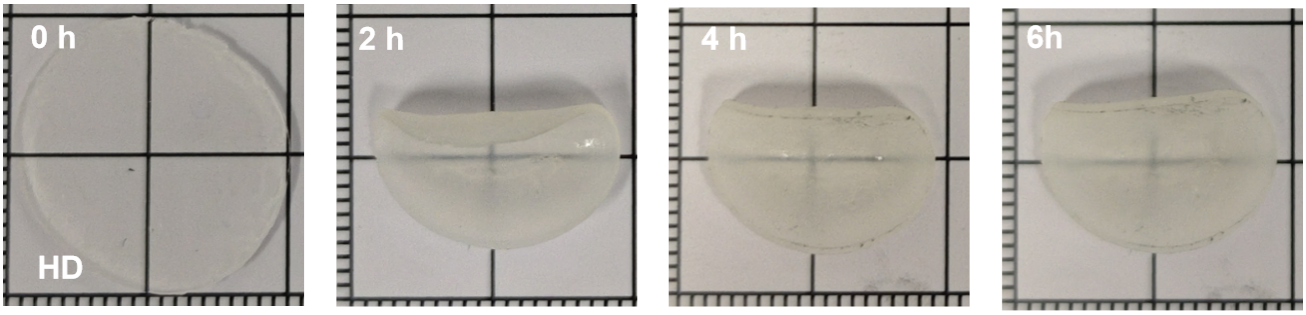


**Figure S9. Optical images of HD electrolytes from 0h to 6 h at 60 °C.**

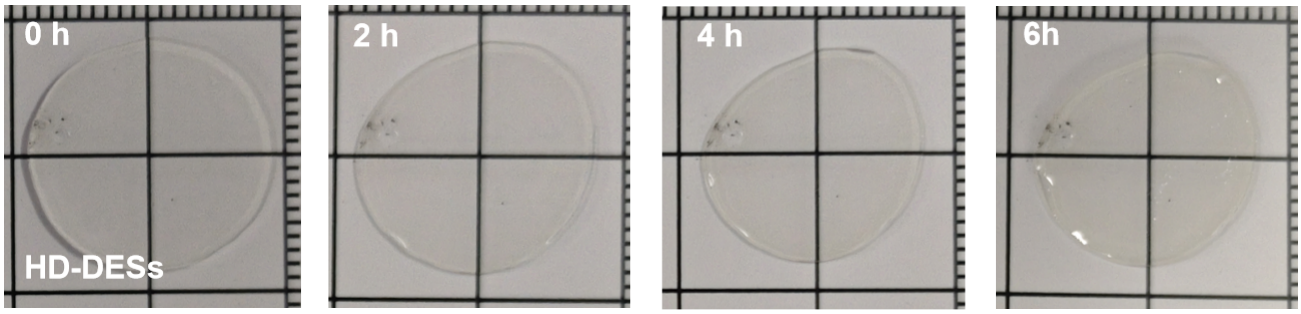


**Figure S10. Optical images of HD-DESs electrolytes from 0h to 6 h at 60 ℃.**

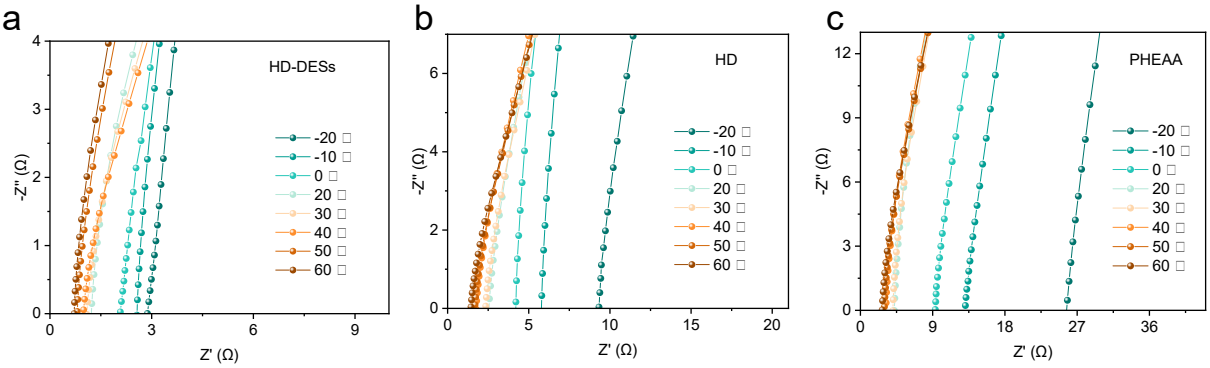


**Figure S11. EIS curves at high frequency of a) HD-DESs, b) HD, and c) PHEAA sandwiched between two stainless steel plates at diffrent temperature.**


**Figure S12.** Digital-micrometer measurement of the HD-DESs gel electrolyte thickness after absorption of the $Zn(OTf)_2$ electrolyte solution. The final electrolyte thickness used for cell assembly was approximately 0.6 mm**.**

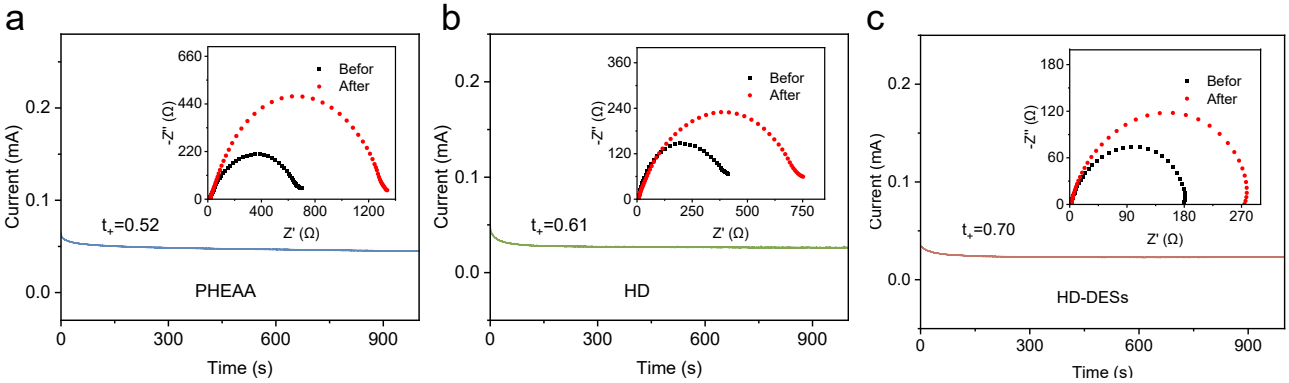


**Figure S13. I-t curve of symmetric cells with a) PHEAA, (b) HD, and (c) HD-DESs.**

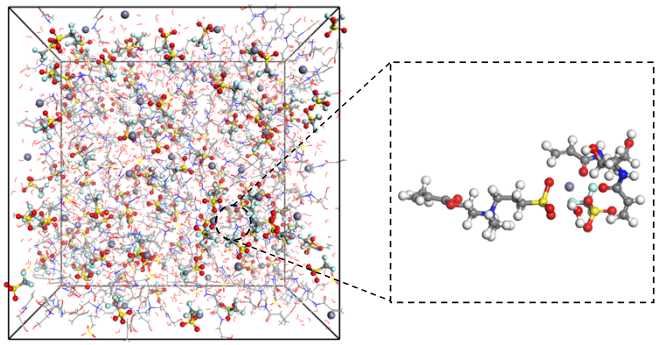

**Figure S14. HD obtained from MD simulations and partially enlarged snapshot representing $Zn^{2+}$ inner solvation structure.**

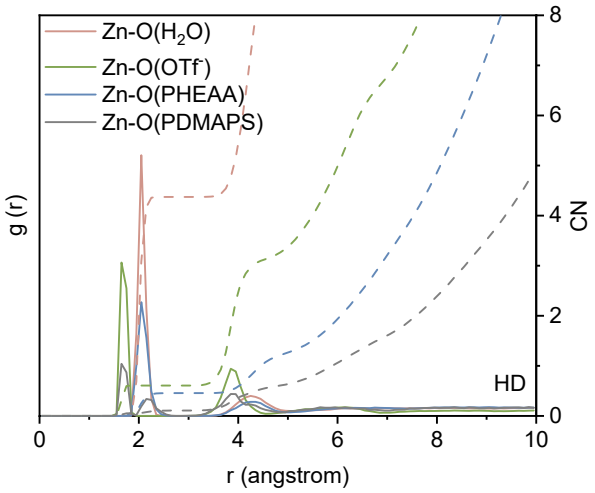


**Figure S15. Radial distribution function (RDF) g(r) and corresponding integrated coordination numbers n(r) of $Zn^{2+}$-O in HD.**

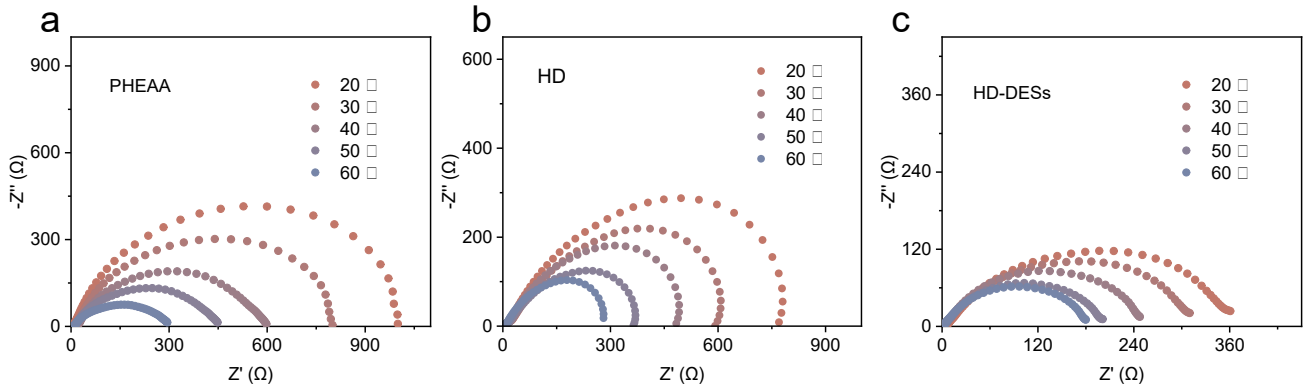


**Figure S16. Temperature-dependent EIS fitting curves of a) PHEAA, (b) HD, and (c) HD-DESs.**

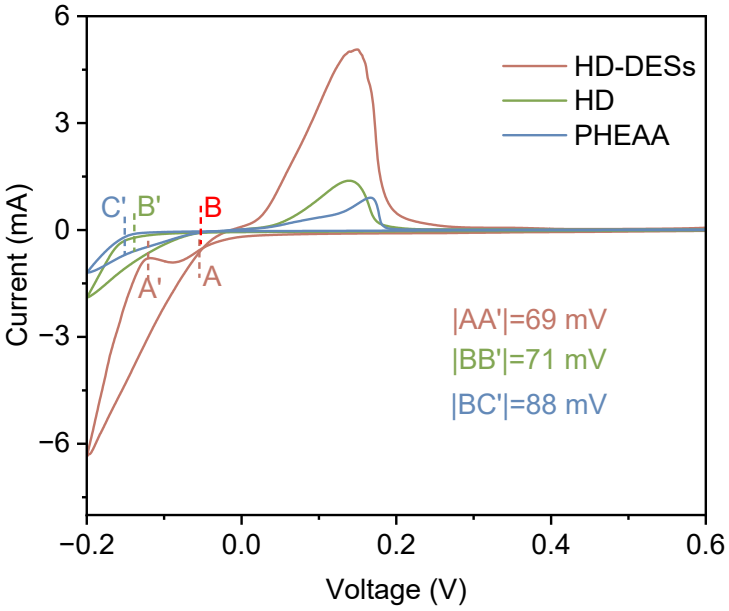


**Figure S17. The CV curves of Zn||Cu half cell.**

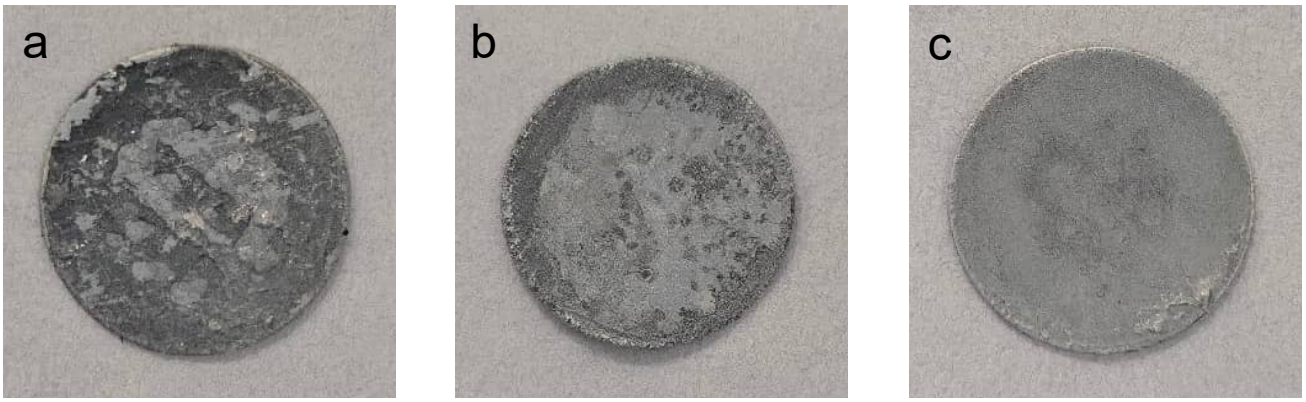


**Figure S18. Optical photographs of zinc anodes after 100 h of cycling in symmetric batteries with (a) PHEAA, (b) HD and (c) HD-DESs electrolyte.**

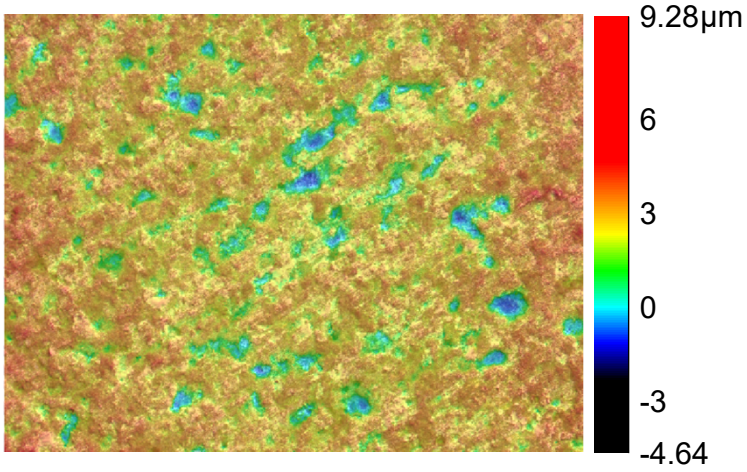


**Figure S19.** LSCM images of Zn anodes after 20 cycles with HD electrolyte.

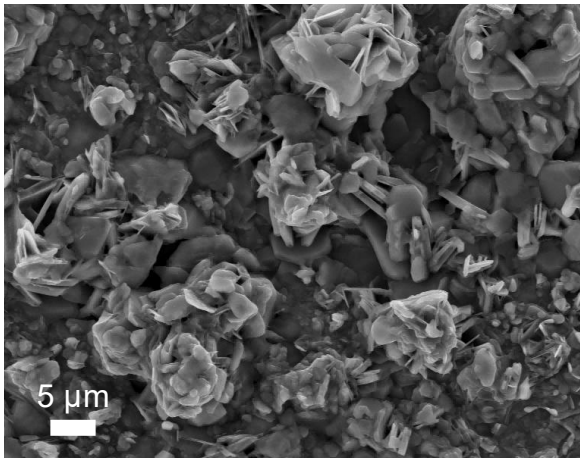


**Figure S20.** SEM images of Zn anodes using HD electrolyte after 20 cycles.

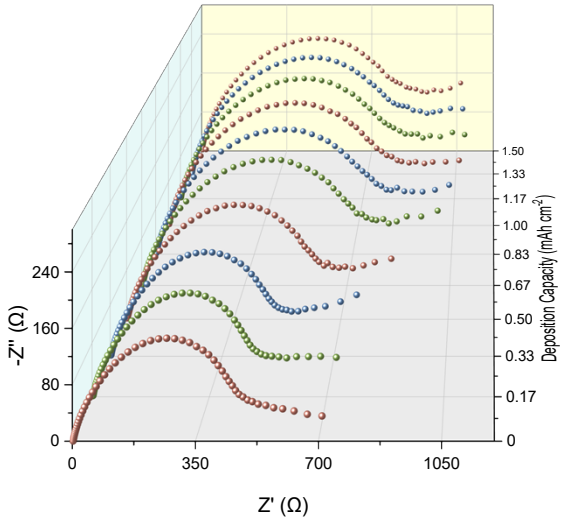


**Figure S21. In situ EIS curves of HD electrolyte.**

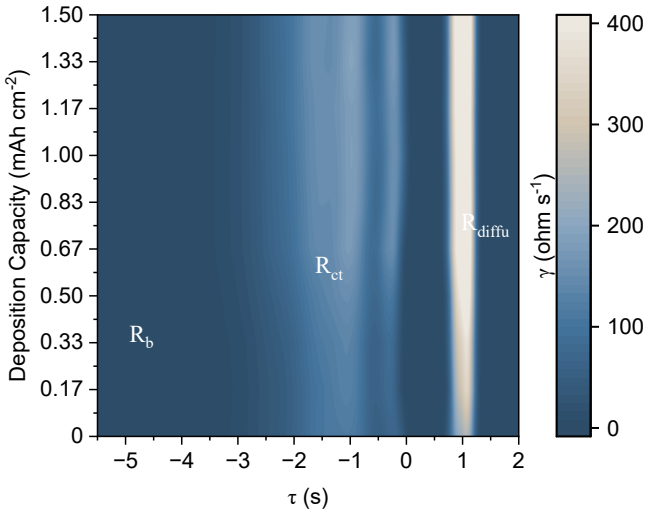


**Figure S22. In situ DRT spectra of symmetric batteries using HD electrolyte.**

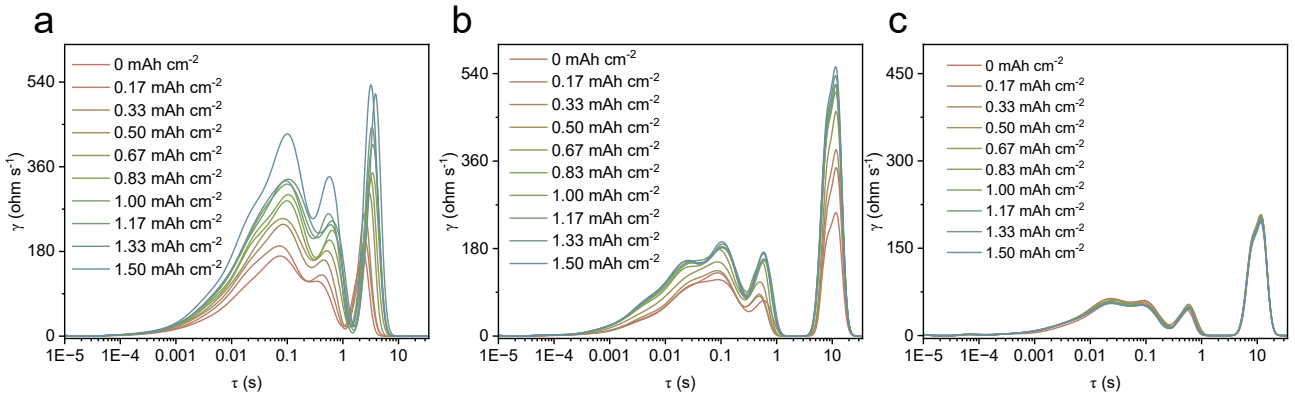


**Figure S23.** In situ DRT line plots of Zn||Zn symmetric cells using (a) PHEAA, (b) HD, and (c) HD-DESs gel electrolytes at different areal capacities during Zn deposition.

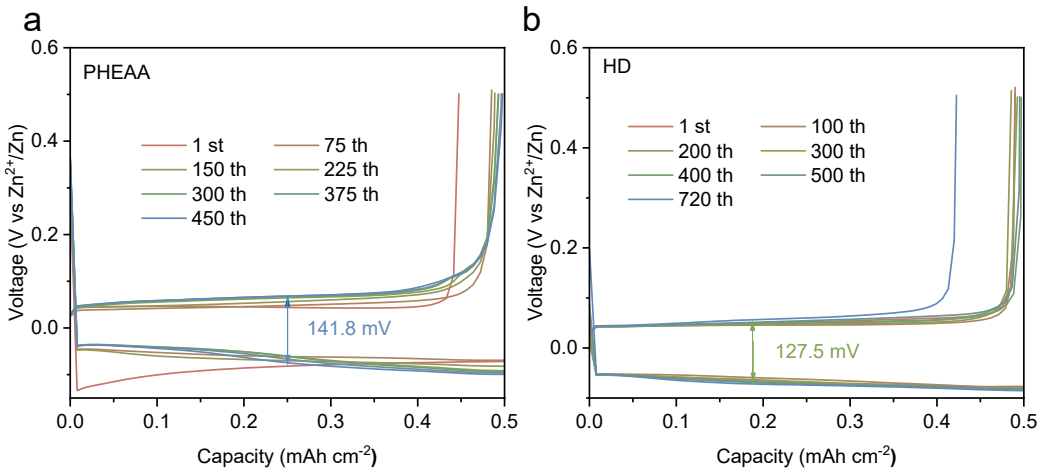


**Figure S24. The capacity-voltage profiles of the Zn||Cu batteries with a) PHEAA and b) HD gel electrolyte at 1 mA cm$^{-2}$ and 0.5 mAh cm$^{-2}$.**

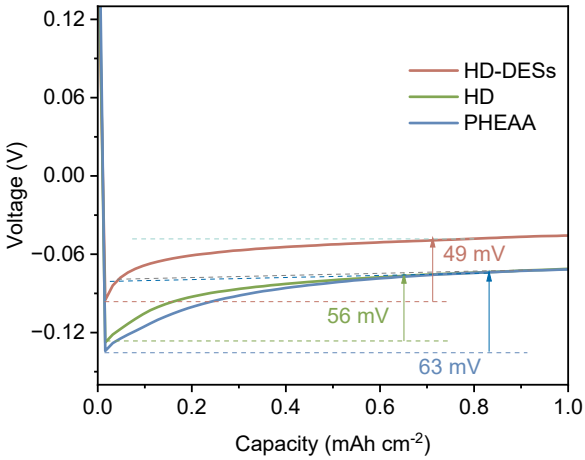


**Figure S25. Zinc-copper half-cell as nuclear power site.**

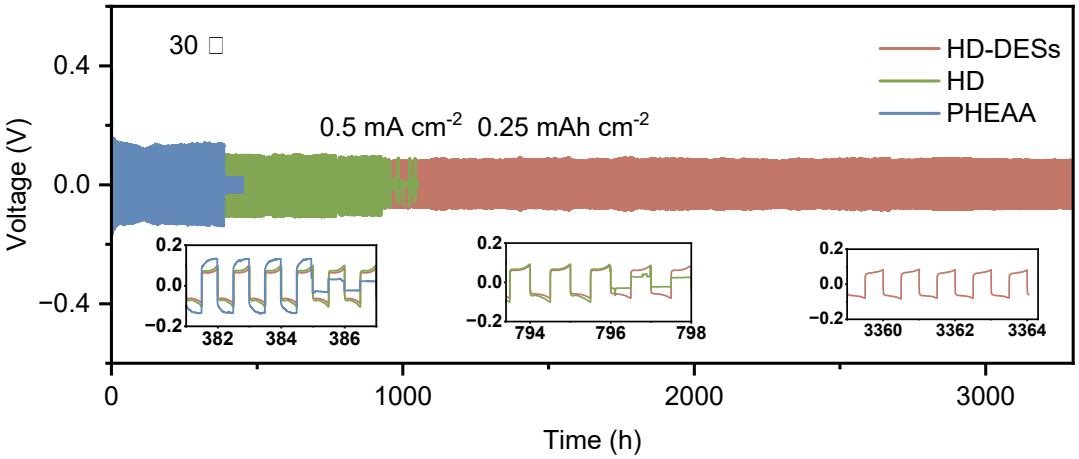


**Figure S26. Cycling performance of Zn||Zn batteries at 0.5mA cm-2, 0.25mAh cm$^{-2}$.**

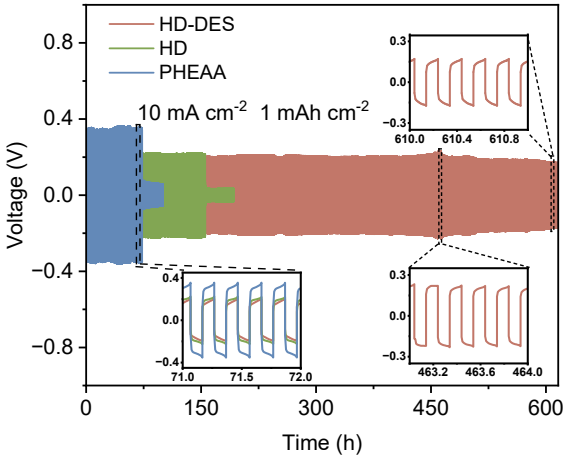


**Figure S27. Cycling performance of Zn||Zn batteries at 10 mA cm$^{-2}$, 1 mAh cm$^{-2}$.**

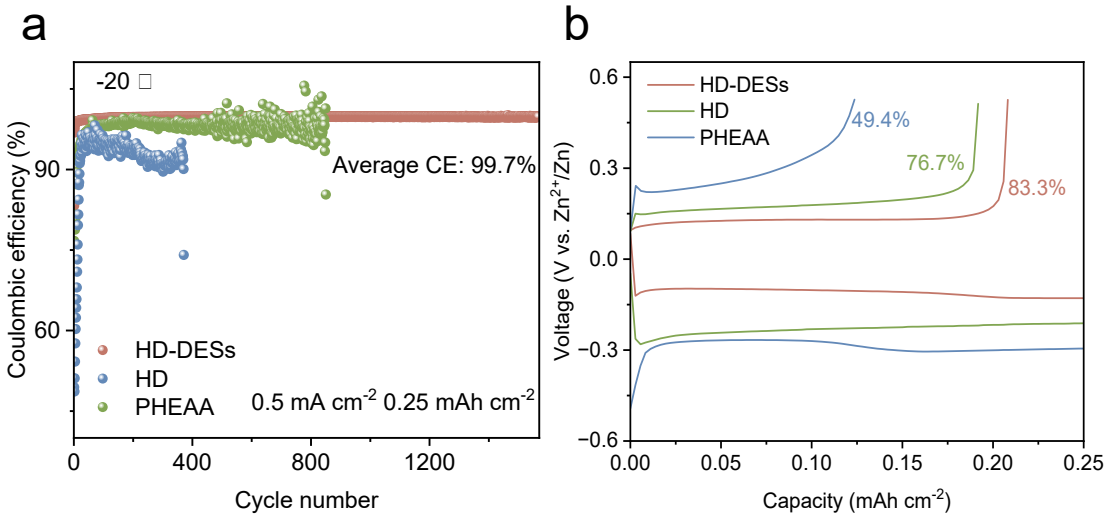


**Figure S28. a)** Coulombic efficiency at -20 ℃ for 0.5 mA $cm^{-2}$, 0.25 mAh $cm^{-2}$, and b) the corresponding cycling curves of the first turn.

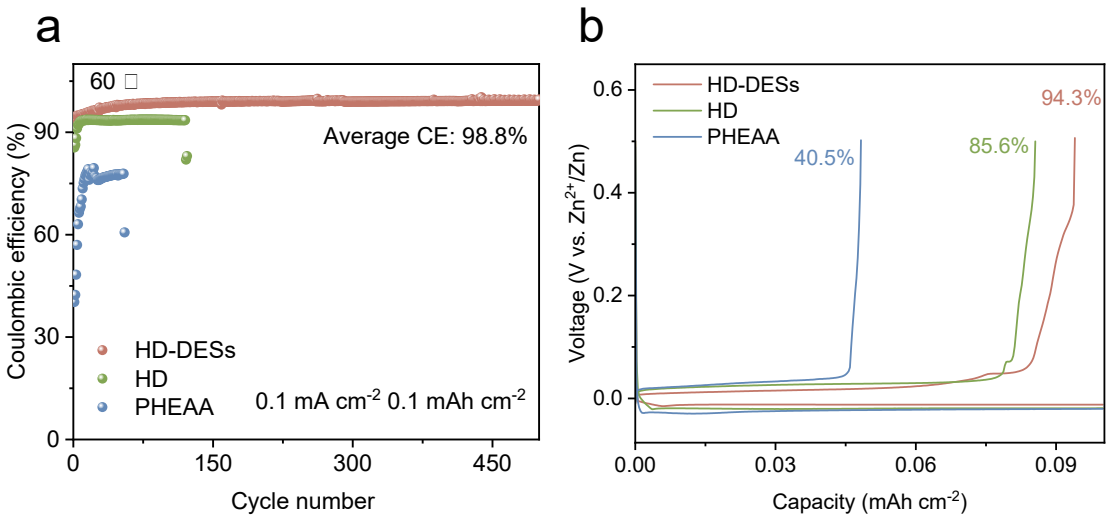


**Figure S29.** Coulombic efficiency at 60 °C for 0.1 mA $cm^{-2}$, 0.1 mAh $cm^{-2}$, and c) the corresponding cycling curves of the first turn.

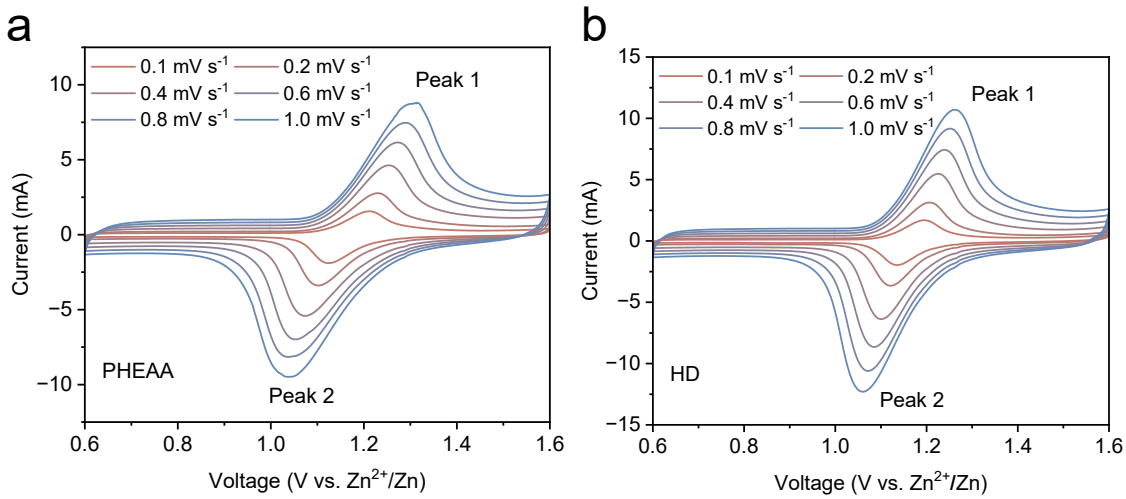


**Figure S30. CV profiles of Zn-$I_2$ cells with a) PHEAA and b) HD electrolyte at different scan rates.**

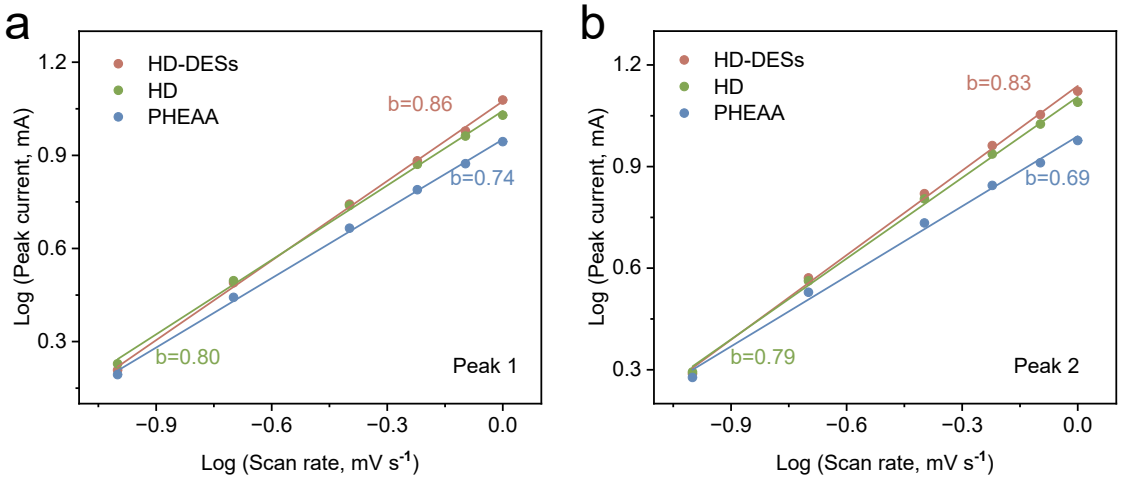


**Figure S31. The corresponding linear relationships between log(peak current) and log(scan rate) for different electrolytes for peak 1 and peak 2.**

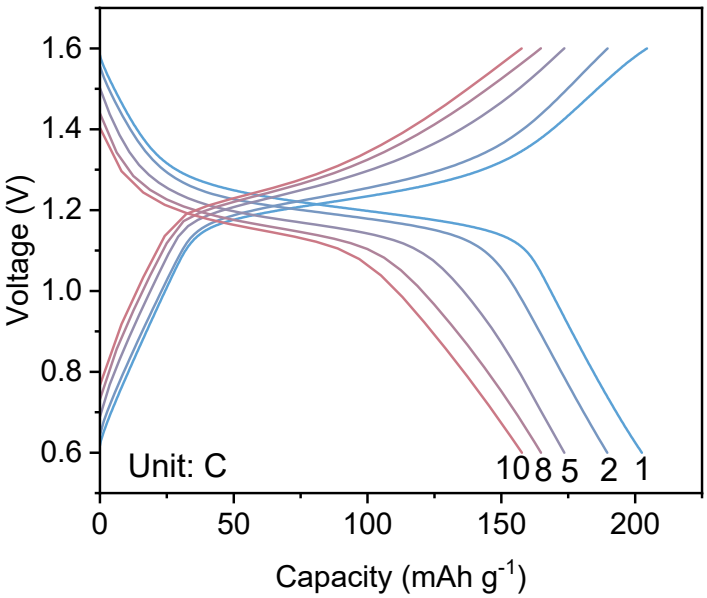


**Figure S32.** The charge-discharge curves of HD gel electrolyte at different current densities.

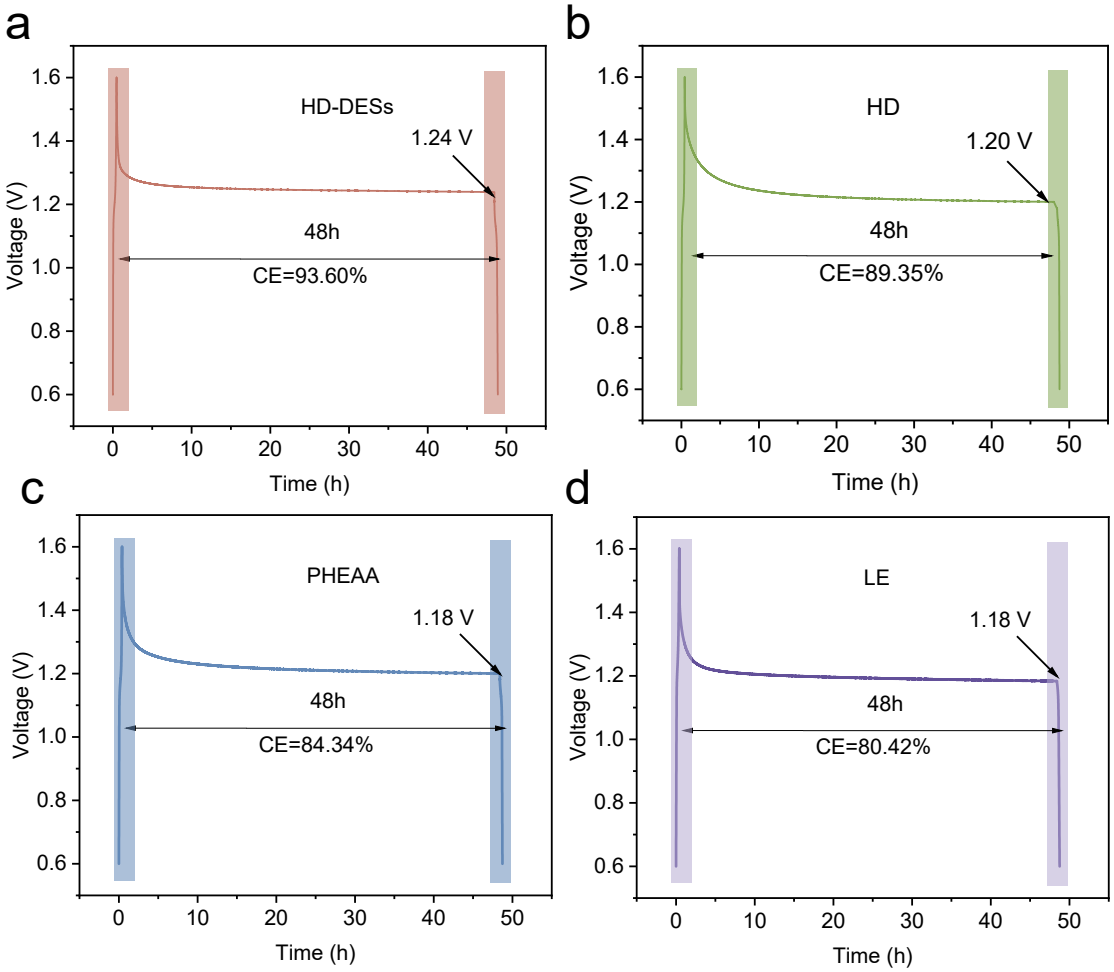


**Figure S33.** Self-discharge curve of a) HD-DESs, b) HD c) PHEAA gel electrolyte and d) LE..

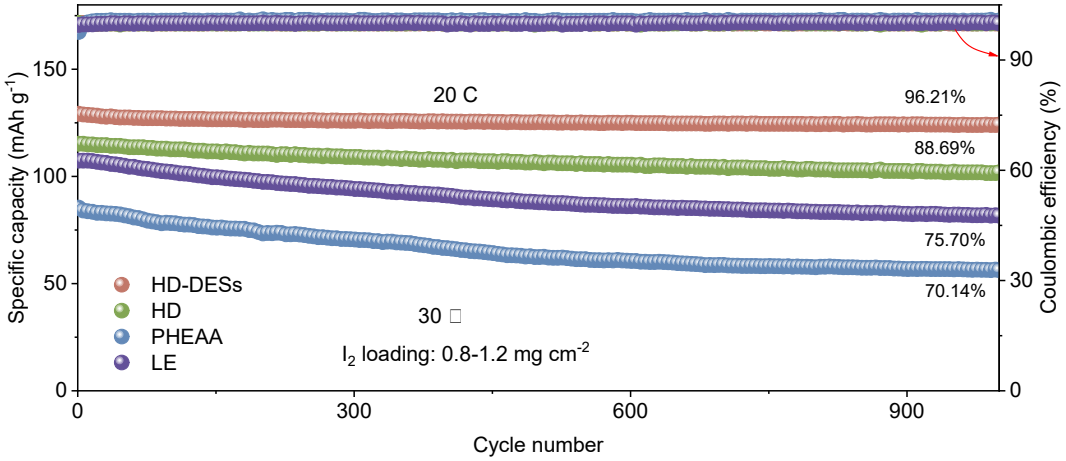


**Figure S34.** Cycling performance of Zn-$I_2$ full cells using PHEAA, HD, HD-DESs, and liquid electrolyte with a commercial separator (LE) at 20 C.

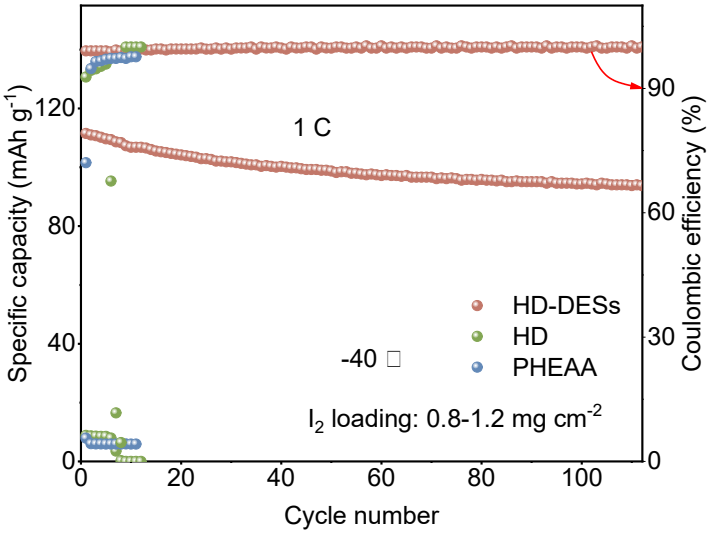


**Figure S35.** Cycling performance at 2 C and −40 °C.

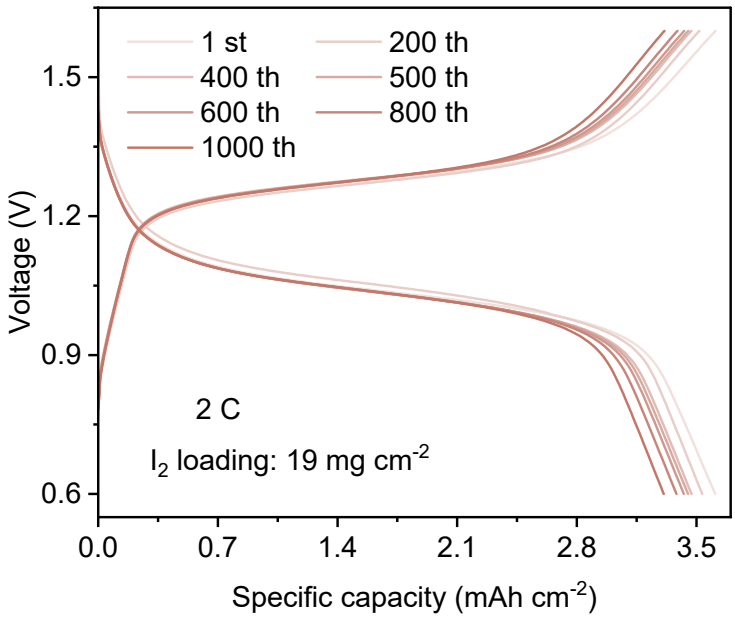


**Figure S36.** The charge-discharge curve of a high-loading AZIBs (19 mg $cm^{-2}$) using the HD-DESs electrolyte.

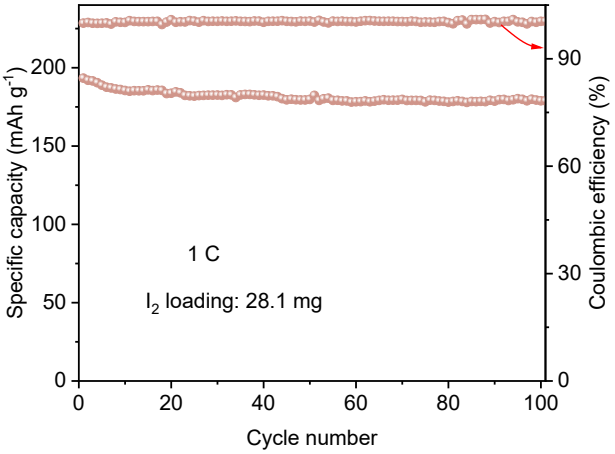


**Figure S37.** Cycling performance of a high-loading AZIBs (28.1 mg cm$^{-2}$) using the HD-DESs electrolyte.

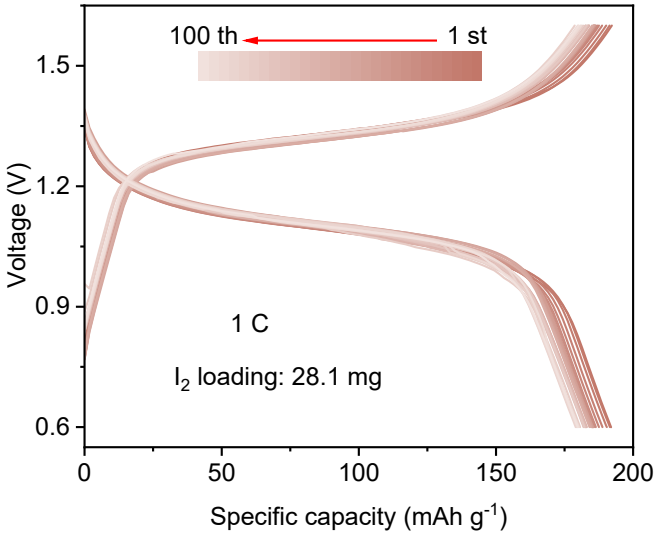


**Figure S38.** The charge-discharge curve of a high-loading AZIBs (28.1 mg cm$^{-2}$) using the HD-DESs electrolyte.

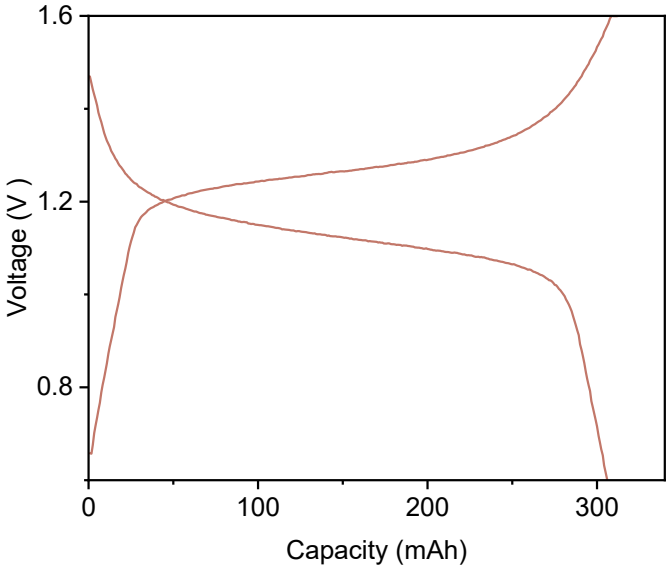


**Figure S39.** Pouch cell charge-discharge curves of HD-DESs gel electrolyte Zn-$I_2$ batteries

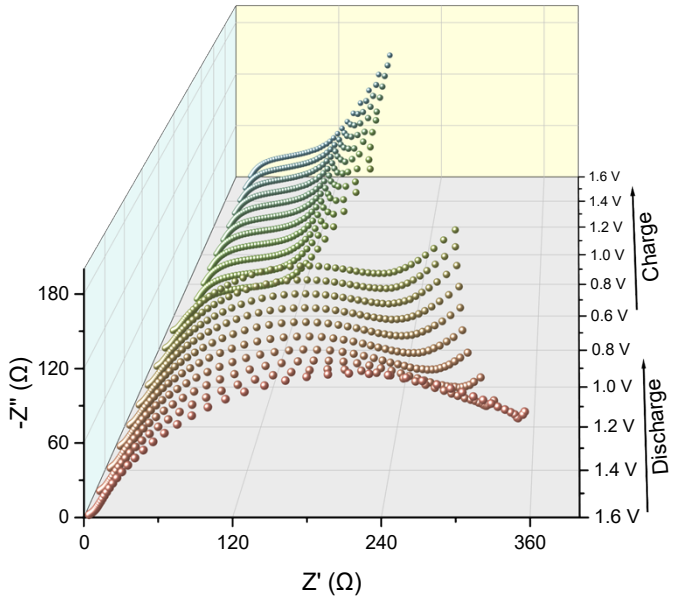


**Figure S40.** In situ EIS curves of Zn-$I_2$ cells with HD electrolyte at different charged and discharged states.

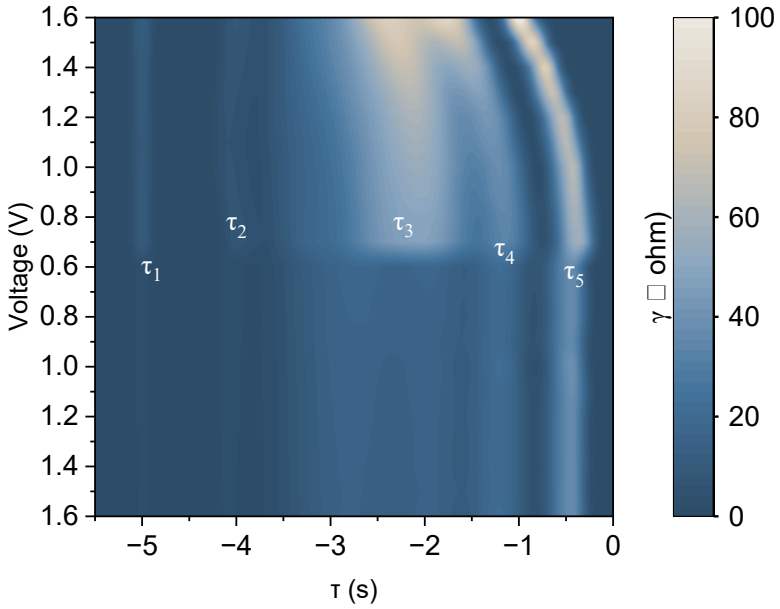


**Figure S41.** in situ DRT spectra of full batteries using HD electrolyte at different charged and discharged states.

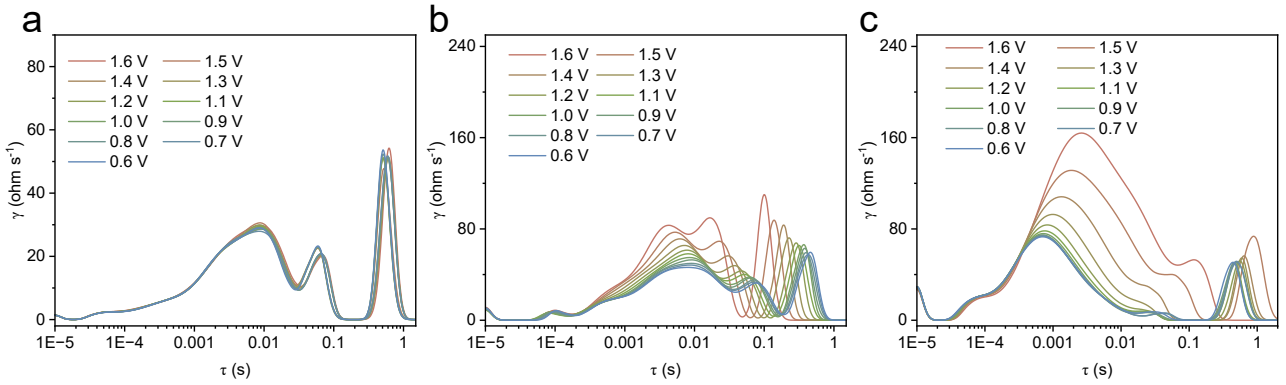


**Figure S42. In situ DRT line plots of Zn-$I_2$ full cells using (a) PHEAA, (b) HD, and (c) HD-DESs gel electrolytes at different voltages during the charge/discharge process.**

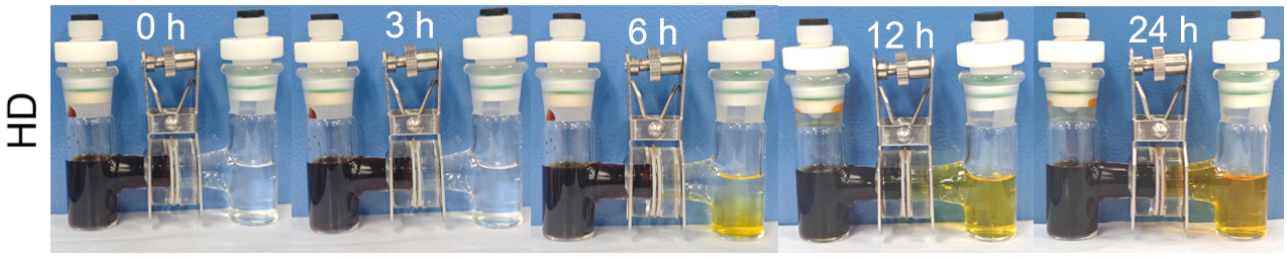


**Figure S43.** Optical images of polyiodide shuttling in H-type cells separated by HD hydrogel.

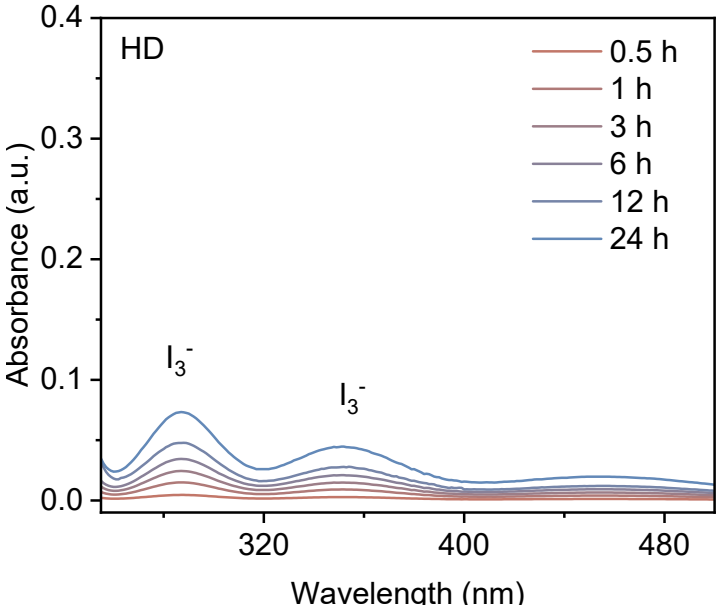


**Figure S44.** UV-vis absorption spectra of the right chamber solutions in the H-type cell with HD hydrogel

**Table S1.** Comparison table of performance for Zn||HD-DESs||Zn symmetric batteries versus other literature-reported zinc anodes protected by different electrolyte.

| Condition | Materials | Current density (mA $cm^{-2}$) | Cycle life (h) | Areal Capacity (mAh $cm^{-2}$) | Ref |
|---|---|---|---|---|---|
| Low temperature | **HD-DESs** | **0.5** | **2300** | **0.5** | **This work** |
| | PAM-T | 1 | 1200 | 1 | [3] |
| | PAM-ZnK4Ac | 0.5 | 1300 | 0.25 | [4] |
| | PZD-20% | 0.1 | 300 | 0.1 | [5] |
| | PAP | 1 | 1200 | 1 | [6] |
| | ZSO/RGSH-0.05 | 0.25 | 580 | 0.25 | [7] |
| | PAM-T-S | 1 | 3000 | 1 | [8] |
| | TSAE | 1 | 400 | 1 | [9] |
| | PSPZ | 0.1 | 320 | 0.1 | [10] |
| | NASHE-0.5 | 1 | 3000 | 0.5 | [11] |
| | BBAS | 1 | 2000 | 1 | [12] |
| Room temperature | **HD-DESs** | **1** | **4000** | **1** | **This work** |
| | PAM-T | 1 | 1200 | 1 | [3] |
| | PAM-ZnK4Ac | 0.5 | 1400 | 0.25 | [4] |
| | PZD-20% | 1 | 1700 | 1 | [5] |
| | ZSO/RGSH-0.05 | 0.25 | 4600 | 0.25 | [7] |
| | HDES10 | 1 | 2700 | 1 | [13] |
| | PAM-T-S | 1 | 3200 | 1 | [8] |
| | PSPZ | 0.1 | 4800 | 0.1 | [9] |
| | NASHE-0.5 | 1 | 1100 | 0.5 | [11] |
| | BBAS | 1 | 2000 | 1 | [12] |
| High temperature | **HD-DESs** | **0.1** | **2700** | **0.1** | **This work** |
| | PAM-T | 1 | 700 | 1 | [3] |
| | PAP | 1 | 2300 | 1 | [6] |

| | | | | |
|---|---|---|---|---|
| ZSO/RGSH-0.05 | 0.25 | 400 | 0.25 | [7] |
| HDES10 | 1 | 2500 | 1 | [13] |
| PAM-T-S | 1 | 810 | 1 | [8] |
| TSAE | 1 | 400 | 1 | [9] |
| PSPZ | 0.1 | 400 | 0.1 | [10] |
| BBAS | 1 | 600 | 1 | [12] |

**Table S2.** Comparison of the battery performance of this work with other literature reports on electrolyte related to AZIB (the capacity decay rate is abbreviated as CDR in this table for convenience).

| Materials | Current density (C) | Cycle number | CDR (‰ per cycle) | Ref |
|---|---|---|---|---|
| **HD-DESs** | **2** | **1450** | **0.0063** | **This work** |
| | **10** | **35000** | **0.0003** | |
| CCH | 2 | 500 | 0.0076 | [14] |
| | 10 | 22000 | 0.0712 | |
| VBC | 5 | 9000 | 0.0025 | [15] |
| | 8 | 18000 | 0.008 | |
| GPZL | 2 | 1000 | 0.0252 | [16] |
| | 10 | 10000 | 0.0067 | |
| skin-QSSE | 5 | 15000 | 0.0072 | [17] |
| | 10 | 45000 | 0.0018 | |
| SBC | 1 | 1000 | 0.0155 | [18] |
| | 8 | 20000 | 0.006 | |
| PAH-PCH | 1 | 2000 | 0.009 | [19] |
| | 8 | 18000 | 0.008 | |

**References**


[1] H. Sun, *The Journal of Physical Chemistry B,* 1998, **102,** 7338-7364.

[2] B. Delley, *Computational Materials Science,* 2000, **17,** 122-126.

[3] L. Wang, H. Wang, J. Cao, J. Yan, C. Dai, W. Sun, Q. Du, Z. Huang, D. Liu, C. Li and J. Sun, *ACS Nano,* 2025, **19,** 28397-28409.

[4] Y. Lin, J. Huang, S. Wang, L. Qi, W. Chen, L. Yu and C. Chen, *Adv. Mater.,* 2025, **37,** e09975.

[5] J. Zhang, C. Lin, L. Zeng, H. Lin, L. He, F. Xiao, L. Luo, P. Xiong, X. Yang, Q. Chen and Q. Qian, *Small,* 2024, **20,** 2312116.

[6] J. Zhong, C. Xia, T. Zhang, H. Wang, H. Tao, C. Lian and Y. Hu, *Adv. Funct. Mater.,* 2025, **36,** e27894.

[7] Y. Chen, S. Zhou, J. Li, X. Zhang, C. Zhou, X. Shi, C. Zhang, G. Fang, S. Liang, Z. Su and A. Pan, *Angew. Chem. Int. Ed.,* 2025, **64,** e202423252.

[8] J. Guan, Y. Mu, X. Wei, L. Yang, Z. Chen, Q. Man, T. Xue, Y. Li, C. Yang, L. Zang and L. Zeng, *Adv. Funct. Mater.,* 2025, **35,** 2508306.

[9] G. Qu, H. Wei, S. Zhao, Y. Yang, X. Zhang, G. Chen, Z. Liu, H. Li and C. Han, *Adv. Mater.,* 2024, **36,** 2400370.

[10] Y. Li, X. Yang, Y. He, F. Li, K. Ouyang, D. Ma, J. Feng, J. Huang, J. Zhao, M. Yang, Y. Wang, Y. Xie, H. Mi and P. Zhang, *Adv. Funct. Mater.,* 2024, **34,** 2307736.

[11] S. Ji, H. Luo, S. Qin, X. Zhang, Y. Hu, W. Zhang, J. Sun, J. Xu, H. Xie, Z. Yan and K. Yang, *Adv. Energy Mater.,* 2024, **14,** 2400063.

[12] Y. Liu, F. Li, J. Hao, H. Li, S. Zhang, J. Mao, T. Zhou, R. Wang, L. Zhang and C. Zhang, *Adv. Funct. Mater.,* 2024, **34,** 2400517.

[13] Z. Chen, W. Zhou, S. Zhao, X. Lou and S. Chen, *Adv. Energy Mater.,* 2025, **15,** 2404108.

[14] J.-L. Yang, T. Xiao, T. Xiao, J. Li, Z. Yu, K. Liu, P. Yang and H. J. Fan, *Adv. Mater.,* 2024, **36,** 2313610.

[15] J. Xu, Y. Zhu, J. Li, X. Chen, P. Zhao, L. Mao and T. Luo, *Chem. Eng. J.,* 2025, **520,** 166041.

[16] C. Wang, X. Du, B. Yang, Z. Tong, H. Zhu, T. Lv, W. Kou, X. Feng and W. Hou, *Chem. Eng. J.,* 2025, **524,** 169040.

[17] S. Cao, A. Zhang, H. Fang, B. Feng, Y. Liu, P. Yi, S. He, Z. Ren, L. Ma, W. Lu, M. Ye and J. Shen, *Energy Environ. Sci.,* 2025, **18,** 3395-3406.

[18] J. Xu, Y. Zhu, Q. Gui, P. Zhao, L. Mao and T. Luo, *Small,* 2025, **21,** e07140.

[19] J.-L. Yang, Z. Yu, J. Wu, J. Li, L. Chen, T. Xiao, T. Xiao, D.-Q. Cai, K. Liu, P. Yang and H. J. Fan, *Adv. Mater.,* 2023, **35,** 2306531.